Journal of Power Sources 196 (2011) 3824–3835

Contents lists available at ScienceDirect

Journal of Power Sources

journal homepage: www.elsevier.com/locate/jpowsour

Performance study of a solid oxide fuel cell and gas turbine hybrid system designed for methane operating with non-designed fuels

Yang Li*, Yiwu Weng

School of Mechanical Engineering, Key Laboratory for Power Machinery and Engineering of Ministry of Education, Shanghai Jiao Tong University, 800 Dong Chuan Rd., Shanghai 200240, China

ARTICLE INFO

Article history:
Received 7 December 2010
Accepted 1 January 2011
Available online 14 January 2011

Keywords:
Solid oxide fuel cell
Gas turbine
Hybrid system
Ethanol
Hydrogen
Methane

ABSTRACT

This paper presents an analysis of the fuel flexibility of a methane-based solid oxide fuel cell-gas turbine (SOFC-GT) hybrid system. The simulation models of the system are mathematically defined. Special attention is paid to the development of an SOFC thermodynamic model that allows for the calculation of radial temperature gradients. Based on the simulation model, the new design point of system for new fuels is defined first; the steady-state performance of the system fed by different fuels is then discussed. When the hybrid system operates with hydrogen, the net power output at the new design point will decrease to 70% of the methane, while the design net efficiency will decrease to 55%. Similar to hydrogen, the net output power of the ethanol-fueled system will decrease to 88% of the methane value due to the lower cooling effect of steam reforming. However, the net efficiency can remain at 61% at high level due to increased heat recuperation from exhaust gas. To increase the power output of the hybrid system operating with non-design fuels without changing the system configuration, three different measures are introduced and investigated in this paper. The introduced measures can increase the system net power output operating with hydrogen to 94% of the original value at the cost of a lower efficiency of 45%.

1. Introduction

High temperature solid oxide fuel cells (SOFCs) seem to be the most efficient device for direct conversion of fuel chemical energy into electricity [1]. Its efficiency can further be increased by integrating it with a gas turbine (GT). This kind of hybrid SOFC-GT power plant is an attractive near-term option, as it can allow efficiencies of over 60%, even for small power outputs (200–400 kW) [2].

In most published papers, methane is the primary fuel for SOFC-GT hybrid systems [3–6]. Methane is the main component of natural gas, which is widely available in densely populated areas. However, it is a fossil fuel with limited resources, and cannot be produced from renewable sources. Thus, the importance of renewable or synthetic fuels is expected to improve during coming decades.

Another issue with natural gas is that it might not be economical to deliver gaseous fuels to sparsely populated, remote areas. Liquid fuels are advantageous due to their higher volumetric energy density, which facilitates trailer distribution and on-site storage. Due to their scalability and efficiency, fuel-cell power plants are considered an interesting option for power supply in sparsely populated, remote areas. In this paper, two alternative fuels are chosen to fuel the hybrid system, namely hydrogen and ethanol. Hydrogen is widely expected to become an important energy carrier in the future because it can be produced from almost any primary energy source with acceptable efficiency. Ethanol is a liquid fuel with high volumetric energy density and can be produced from biomass.

Thus, it is important to determine whether an SOFC-GT hybrid system designed for methane fuel can be easily modified to other fuel sources once the focus turns from natural gas to other renewable, novel gases. In recent years, many researchers have studied the feasibility of SOFC operating on biogas or other suitable fuels such as ethanol and methanol [7–9]. Most hold the opinion that such fuels can be directly fed and internally reformed in an SOFC stack. Laboratory tests performed by Jenner et al. confirmed that the efficiency of SOFC drops by approximately 5% when the mole fraction of methane in the fuel decreases from 70 to 30% [10]. Yi et al. showed that the electrical efficiency of an integrated SOFC drops around 1.1% if biogas is used instead of natural gas [11]. Bo Huang et al. fabricated a single cell of SOFC and tested its electrochemical performance fed by ethanol steam [12]. Few papers have focused on the necessary modification and performance of SOFC-GT hybrid system operating with non-designed fuels.

This paper discusses the performance of a methane-based SOFC-GT hybrid system operating with non-designed fuels. Detailed simulation models of all components of the system are mathemat-

* Corresponding author. Tel.: +86 21 34206342; fax: +86 21 34206342.
E-mail address: yli2350@gmail.com (Y. Li).

0378-7753/$ – see front matter © 2011 Elsevier B.V. All rights reserved.
doi:10.1016/j.jpowsour.2011.01.011

Nomenclature

A_{el}	active surface of fuel cell (m^2)
A	surface
C_{PR}	specific internal energy ($kJ\,kg^{-1}$)
c	heat capacity ($J\,kg^{-1}\,K$) or mole concentrations of species
F	Faraday constant (C) or molar flow rate ($mol\,s^{-1}$)
G	gas flow rate ($kg\,s^{-1}$)
h	heat transfer coefficient ($W\,m^{-2}\,K^{-1}$) or specific enthalpy ($kJ\,kg^{-1}$)
Δh	enthalpy change of the reaction ($J\,mol^{-1}$)
K	equilibrium constant of reaction
k	thermal conductivity($W\,K^{-1}\,m^{-1}$)
I	current density ($A\,m^{-2}$)
l	tube length
$\dot{m}$	flow rate
P	pressure (Pa) or power density ($W\,m^{-2}$)
p	partial pressure (Pa)
$\dot{q}$	radiation heat flow (W)
R	gas constant ($J\,mol^{-1}\,K^{-1}$) or resistance (Ω)
r	radius (m)
$\dot{r}$	reaction rate ($mol\,s^{-1}$)
T	temperature (K)
U	voltage (V)
u	flow velocities ($m\,s^{-1}$)
W	power
x	mole fraction

Greek symbols

η	efficiency
ρ	density ($kg\,m^{-3}$) or ohmic resistance ($\Omega\,m$)
ε	compression pressure ratio
δ	expansion pressure ratio or thickness (m)

Subscripts

ADT	air delivery tube
c	compressor
Fu	fuel
f	fuel channel
MEA	membrane electrolyte assembly
op	over potential
ocp	open circuit potential
Ref	reforming reaction
Shi	water–gas shift reaction
T	turbine

ically defined, paying more attention to the SOFC thermodynamic model developed. Based on the simulation models, the feasibility and steady-state performance of a methane-based SOFC-GT hybrid system operating with hydrogen and ethanol are discussed. Three different methods are introduced to increase the power output of a hybrid system operating with non-designed fuel.

2. Mathematical models

2.1. System configurations

The SOFC-GT hybrid system configuration is shown in Fig. 1. The steam required to support reforming reactions (reactions (I) and (II) in Table 1) is derived from the anode outlet stream. During the start-up procedure, the plant requires an external boiler that produces steam for the reforming reaction. In this paper, the startup procedure is not taken into account; thus, the external boiler is not

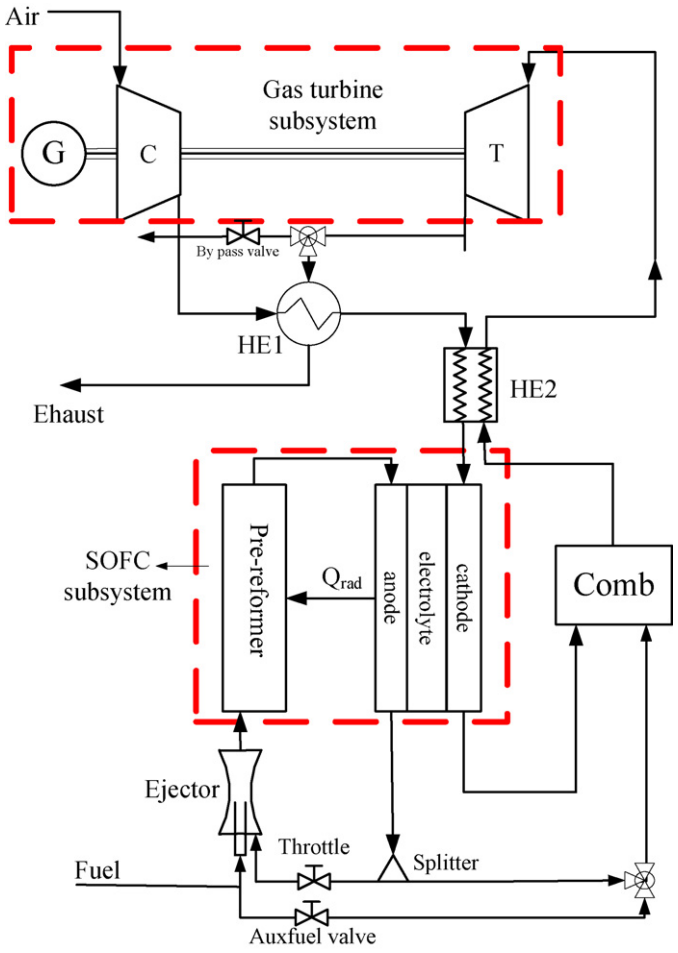

Fig. 1. Configurations of SOFC-GT hybrid system.

considered. The hybrid system mainly includes an SOFC subsystem, a gas turbine subsystem, two exchangers, a combustor, and a pre-reformer. The working principle of the plant can be summarized as follows.

The compressed air is preheated through two heat exchangers (HE1 and HE2) before entering the cathode of the SOFC stack. In the anode compartment, fuel is mixed with anode re-circulated stream before entering the pre-former. After being preheated and partly reformed in the pre-reformer, it is carried to the external surface of the SOFC tube, where internal reformation occurs, releasing hydrogen, which is brought to three-phase boundaries (TPBs) [13]. Preheated air is fed to the top of the stack, where is further preheated and finally carried, by air delivery tube (ATD), into the SOFC tube as shown in Fig. 2. There, it participates in the cathode electrochemical semi-reaction. The electrochemical reactions occur at the TPB of both electrodes, producing an ionic flow through the electrolyte and electron across the electrodes. Electrical energy is hence produced associated with heat generation during the process. The heat generated is partly used to reform the fuels, partly dissipated to the environment, and partly used to heat up the feedstock gases. The excess air and unreacted fuels are burnt within the combustor

Table 1
Reactions in SOFC tube.

Steam reforming reaction	$CH_4 + H_2O \Leftrightarrow 3H_2 + CO$	(I)
	$C_2H_5OH + 3H_2O \Leftrightarrow 2CO_2 + 6H_2$	(II)
Water gas shift reaction	$CO{+}H_2O \Leftrightarrow CO_2{+}H_2$	(III)
Oxidation	$H_2{+}O^{2-} \rightarrow H_2O{+}2e^-$	(IV)
Reduction	$O_2{+}4e^- \rightarrow 2O^{2-}$	(V)

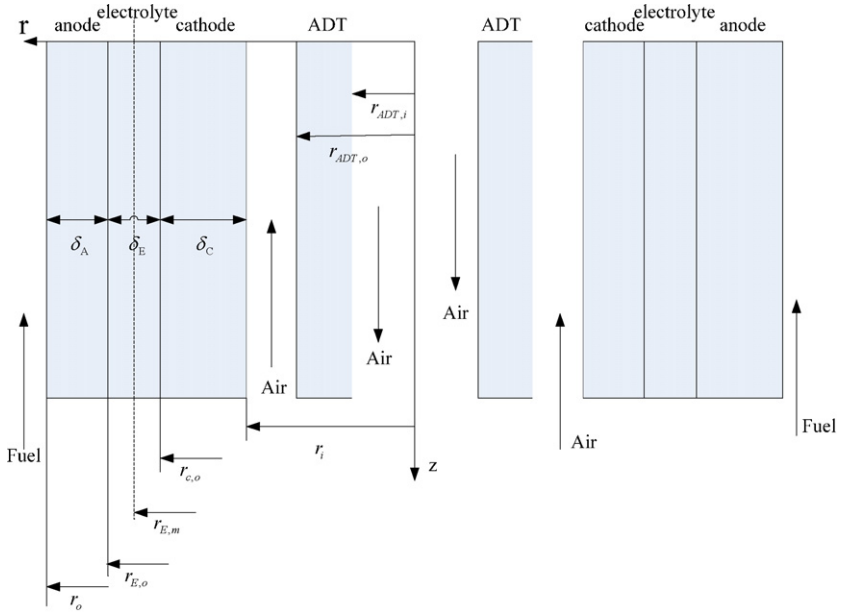

Fig. 2. Geometric profile of SOFC tube.

to increase stream temperature partly. HE2 is placed before the GT inlet to preheat the SOFC inlet air. The high temperature-pressured gas then expands in the turbine and produces mechanical work to drive the air compressors and the directly coupled electrical generator.

2.2. SOFC model

The SOFC model developed in this study is based on a tubular design. The geometry of the SOFC is based on the design of Siemens-Westinghouse [14,15]; the geometric profile is shown in Fig. 2. The model developed in this paper is based on the following assumptions.

1. The model described a bundle of non-interacting fuel cell tubes, no stack effects are considered.
2. The gas flows are modeled as plug flows.
3. Laminar flow is assumed in heat transfer models.
4. The shift reaction is assumed to be always at equilibrium.
5. All heat sources and sinks derived from the reactions attack at the anode surface.

The SOFC model presented in this paper consists of both electrochemical and thermal models. The thermodynamic model includes convectional heat transfer between gases and solids as well as radiation and conduction between solid materials is developed, allowing for the calculation of radial temperature gradients. Kinetics of reforming and electrochemical reactions is included in the electrochemical model.

2.2.1. Electrochemical reactions

In an SOFC, the electric power is generated through the following reactions as shown in Table 1.

The reaction rate of the CH_4 reforming reaction (I) is determined by:

$$\dot{r}_{Ref(I)}(z) = k_{act} \cdot e^{-(E_{act})/(R \cdot T_{MEA}(r_{E,m},z))} \cdot x_{Fu}(z, CH_4) \cdot P_{Fu,ref} \cdot A_{el} \quad (1)$$

where E_{act} is the activation energy while k_{act} is the pre-exponential constant.

The value of E_{act} and k_{act} have been given in Ref. [16] $E_{act} = 82 \times 10^3$ J mol^{-1}; $k_{act} = 0.04274$ mol s^{-1} m^{-2} Pa^{-1}. Such formation is considered typically for the DIR-SOFC performance.

C_2H_5OH reforming reaction is much more complex than that of CH_4 which has been described in many papers such as [17]. The ethanol reforming reaction kinetic model derived by Abayomic Akande are adopted in this paper. The model is of the form

$$\dot{r}_{Ref(II)}(z) = k_0 \cdot x^n(z, C_2H_5OH) \cdot e^{-(E_0)/(R \cdot T_{MEA}(r_{E,m},z))} P_{Fu,ref} \cdot A_{el} \quad (2)$$

where k_0 is the pre-exponential constant; E_0 is the activation energy; n is the order of reaction with respect to ethanol. The value of E_{act}, n and k_{act} have been given based on experimental data in Ref. [18], in which $k_0 = 3.12 \times 10^{-2}$; $n = 0.43$; $E_0 = 4.41 \times 10^3$.

The reaction rate of the shift reaction can be calculated by:

$$\dot{r}_{Shi}(z) = 10^4 \left(x_{Fu}(z, CO) \cdot x_{Fu}(z, CO) - \frac{x_{Fu}(z, H_2) \cdot x_{Fu}(z, CO_2)}{K_{Shi}(z)} \right); \quad \times \quad z \in [0, l) \quad (3)$$

where $K_{Shi}(z)$ is the equilibrium constant and can be calculated by: $(4) \ln(K_{Shi}(z)) = -\frac{g^0(H_2)+g^0(CO_2)-g^0(CO)-g^0(H_2O)}{R_m T_{MEA}(r_{E,m},z)}$

The electrochemical reaction rate is calculated from the distributed current density.

$$\dot{r}_{Elc}(z) = \frac{I(z) \cdot A_{el}}{2 \cdot F} \quad (5)$$

2.2.2. Heat transfer and radiation

Both fuel reforming and water–gas shift reactions are endothermic, and the required heat of the reactions is calculated by:

$$\Delta h_{Ref(I)}(z) = 3 \cdot (0 + h(H_2)) + (h_f^0(CO) + h(CO)) - (h_f^0(CH_4) + h(CH_4)) - (h_f^0(H_2O) + h(H_2O)) \quad (6)$$

$$\Delta h_{Ref(II)}(z) = 4 \cdot (0 + h(H_2)) + 2 \cdot (h_f^0(CO) + h(CO)) - (h_f^0(C_2H_5OH) + h(C_2H_5OH)) - (h_f^0(H_2O) + h(H_2O)) \quad (7)$$

$$\Delta h_{Shi}(z) = 3 \cdot (0 + h(H_2)) + (h_f^0(CO) + h(CO)) - (h_f^0(CO) + h(CO)) - (h_f^0(H_2O) + h(H_2O)) \quad (8)$$

For the electrochemical reaction, part of the enthalpy change is turned into electric power.

$$\Delta h_{\mathrm{Elc}}(z) = (h_{\mathrm{f}}^0(\mathrm{H_2O}) + h(\mathrm{H_2O})) - \frac{1}{2}(h_{\mathrm{f}}^0(\mathrm{O_2}) + h(\mathrm{O_2})) - (0 + h(\mathrm{H_2})) + 2 \cdot U \cdot F \tag{9}$$

The boundary heat transfer between the ADT and ADT air is calculated by:

$$k_{\mathrm{ADT}} \cdot \frac{\partial T_{\mathrm{ADT}}(r_{\mathrm{ADT},i}, z)}{\partial r_{\mathrm{ADT}}} = h_{\mathrm{c,ADTAir-ADT}}(z) \cdot (T_{\mathrm{ADT}}(r_{\mathrm{ADT},i}, z) - T_{\mathrm{ADTAir}}(z)); \quad z \in (0, l) \tag{10}$$

The heat conduction in the radial and axial direction inside the ADT is:

$$c_{\mathrm{ADT}} \cdot \rho_{\mathrm{ADT}} \cdot \frac{dT_{\mathrm{ADT}}(r, z)}{dt} = k_{\mathrm{ADT}} \cdot \left(\frac{\partial^2 T_{\mathrm{ADT}}(r, z)}{\partial z_{\mathrm{c}}^2} + \frac{\partial(r \cdot \partial T_{\mathrm{ADT}}(r, z))}{r \cdot \partial r_{\mathrm{ADT}}^2} \right); \quad \times \quad r \in (r_{\mathrm{ADT},i}, r_{\mathrm{ADT},o}), \quad z \in (0, l) \tag{11}$$

The boundary heat transfer between ADT and cathode air (including radiation from the cathode surface) is calculated by:

$$k_{\mathrm{ADT}} \cdot \frac{\partial T_{\mathrm{ADT}}(r_{\mathrm{ADT},i}, z)}{\partial r_{\mathrm{ADT}}} = -h_{\mathrm{c,Air-ADT}}(z) \cdot (T_{\mathrm{ADT}}(r_{\mathrm{ADT},o}, z) - T_{\mathrm{Air}}(z)) + \frac{\dot{q}_{\mathrm{C-ADT}}(z)}{2\pi r_{\mathrm{ADT},o} l} \tag{12}$$

The heat transport in the cathode air is calculated by:

$$\sum_{i=1}^{7} c_{\mathrm{Air}}(z, i) \cdot c_{\mathrm{p,Air}}(z) \cdot \left(\frac{dT_{\mathrm{Air}}(z)}{dt} + u_{\mathrm{Air}}(l) \cdot \frac{\partial T_{\mathrm{Air}}(z)}{\partial z_{\mathrm{f}}} \right) = \frac{2 \cdot r_{\mathrm{ADT},o}}{r_i^2 - r_{\mathrm{ADT},o}^2} \cdot h_{\mathrm{c,Air-ADT}}(z) \cdot (T_{\mathrm{ADT}}(r_{\mathrm{ADT},o}, z) - T_{\mathrm{Air}}(z)) + \frac{2 \cdot r_i}{r_i^2 - r_{\mathrm{ADT},o}^2} \cdot h_{\mathrm{c,Air-C}}(z) \cdot (T_{\mathrm{MEA}}(r_{i,z}) - T_{\mathrm{Air}}(z)), \quad \times \quad z \in (0, l) \tag{13}$$

The boundary heat transfer between cathode air and cathode (including ratio to the ADT surface) is calculated by:

$$k_{\mathrm{MEA,r}} \cdot \frac{\partial T_{\mathrm{MEA}}(r_i, z)}{\partial r_{\mathrm{MEA}}} = -h_{\mathrm{c,Air-C}}(z) \cdot (T_{\mathrm{MEA}}(r_i, z) - T_{\mathrm{Air}}(z)) + \frac{\dot{q}_{\mathrm{C-ADT}}(z)}{2\pi r_i l} \tag{14}$$

where $\dot{q}_{\mathrm{C-ADT}}(z)$ is the radiation heat flow between the cathode and the ADT, which can be calculated by:

$$\dot{q}_{\mathrm{C-ADT}}(z) = \tau_{\mathrm{C-ADT}} \cdot \sigma_{\mathrm{B}} \cdot (T_{\mathrm{MEA}}(r_i, z)^4 - T_{\mathrm{ADT}}(r_{\mathrm{ADT},o}, z)^4) \tag{15}$$

The heat transfer in the radial and axial directions inside the MEA (note different heat conductivities in the radial and axial directions) is calculated by:

$$\frac{dT_{\mathrm{MEA}}(r, z)}{dt} = k_{\mathrm{MEA,z}} \cdot \frac{\partial^2 T_{\mathrm{MEA}}(r, z)}{\partial z_{\mathrm{c}}^2} + k_{\mathrm{MEA,r}} \cdot \frac{\partial(r \cdot \partial T_{\mathrm{ADT}}(r, z))}{r \cdot \partial r_{\mathrm{ADT}}^2} \quad \times \quad r \in (r_i, r_o), \quad z \in (0, l) \tag{16}$$

The boundary heat transfer between the anode and the fuel (including heat of the reaction and radiation to the reformer and the casing) is calculated by:

$$k_{\mathrm{MEA,r}} \cdot \frac{\partial T_{\mathrm{MEA}}(r_o, z)}{\partial r_{\mathrm{MEA}}} = -h_{\mathrm{c,Fu-A}}(z) \cdot (T_{\mathrm{MEA}}(r_o, z) - T_{\mathrm{Fu}}(z)) - \frac{\dot{r}_{\mathrm{Ref}} \Delta h_{\mathrm{Ref}} + \dot{r}_{\mathrm{Shi}} \Delta h_{\mathrm{Shi}} + \dot{r}_{\mathrm{Elc}} \Delta h_{\mathrm{Elc}} + \dot{q}_{\mathrm{rad,Ref}}(z) + \dot{q}_{\mathrm{rad,Cas}}(z)}{2\pi r_o l} \tag{17}$$

where $\dot{q}_{\mathrm{rad,Ref}}(z)$ and $\dot{q}_{\mathrm{rad,Cas}}(z)$ are the radiation heat flows from the anode surface to the reformer and the anode surface to the stack casing, respectively:

$$\dot{q}_{\mathrm{Ref}}(z) = \tau_{\mathrm{Ref}} \cdot \sigma_{\mathrm{B}} \cdot (T_{\mathrm{e,Ref}}(z)^4 - T_{\mathrm{r,Ref}}(z)^4) \tag{18}$$

$$\dot{q}_{\mathrm{Rad,cas}}(z) = \tau_{\mathrm{Cas}} \cdot \sigma_{\mathrm{B}} \cdot (T_{\mathrm{e,Cas}}(z)^4 - T_{\mathrm{r,Cas}}(z)^4) \tag{19}$$

The heat transport in the fuel is calculated by:

$$\sum_{i=1}^{7} c_{\mathrm{Fu}}(z, i) \cdot c_{\mathrm{p,Fu}}(z) \cdot \left(\frac{dT_{\mathrm{Fu}}(z)}{dt} + u_{\mathrm{Fu}}(l) \cdot \frac{\partial T_{\mathrm{Fu}}(z)}{\partial z_{\mathrm{f}}} \right) = \frac{2\pi \cdot r_o}{A_{\mathrm{Fu}}} \cdot h_{\mathrm{c,Fu-A}}(z) \cdot (T_{\mathrm{MEA}}(r_o, z) - T_{\mathrm{Fu}}(z)), \quad \times \quad z \in (0, l) \tag{20}$$

Assuming $r_o - r_i \ll r_i$, the mean temperature over the MEA can be calculated by.

$$T_{\mathrm{MEA,mean}} = \frac{1}{l \cdot (r_o - r_i)} \int_{z=0}^{l} \int_{r=r_i}^{r_o} T_{\mathrm{MEA}}(r, z) dr dz \tag{21}$$

The local heat gradient maxima in the radial of the MEA were calculated by:

$$dTdr_{\mathrm{MEA,max}} = \max \left(\frac{\partial T_{\mathrm{MEA}}(r, z)}{\partial r_{\mathrm{MEA}}} \right) \tag{22}$$

2.2.3. Mass transfer model

On the air side, there is only one sink term exit for oxygen, and no source or sink terms exit for other components.

$$\frac{dc_{\mathrm{Air}}(z, \mathrm{O_2})}{dt} + u_{\mathrm{Air}}(l) \frac{\partial c_{\mathrm{Air}}(z, \mathrm{O_2})}{\partial z_{\mathrm{c}}} = \frac{(-1/2)\dot{r}_{\mathrm{Elc}}(z)}{l \cdot (r_i^2 - r_{\mathrm{ADT},o}^2)\pi} \quad \forall \quad z \in [0, l) \tag{23}$$

$$\frac{dc_{\mathrm{Air}}(z, i)}{dt} + u_{\mathrm{Air}}(l) \frac{\partial c_{\mathrm{Air}}(z, i)}{\partial z_c} = 0 \quad z \in [0, l), \quad i \in \{\mathrm{N_2}, \mathrm{H_2}, \mathrm{CH_4}, \mathrm{CO}, \mathrm{H_2O}, \mathrm{CO_2}, \mathrm{C_2H_5OH}\} \tag{24}$$

On the fuel side, there is no source or sink terms exit for nitrogen or oxygen.

$$\frac{dc_{\mathrm{Fu}}(z, i)}{dt} + u_{\mathrm{Fu}}(l) \frac{\partial c_{\mathrm{Fu}}(z, i)}{\partial z_c} = 0; \quad z \in [0, l), \quad i \in \{\mathrm{N_2}, \mathrm{O_2}\} \tag{25}$$

The mass transfer equations for other species are:

$$\frac{dc_{\mathrm{Fu}}(z, \mathrm{H_2})}{dt} + u_{\mathrm{Fu}}(l) \frac{\partial c_{\mathrm{Fu}}(z, \mathrm{H_2})}{\partial z_{\mathrm{c}}} = \frac{3\dot{r}_{\mathrm{Ref(I)}}(z) + 4\dot{r}_{\mathrm{Ref(I)}}(z) + \dot{r}_{\mathrm{Shi}}(z) - \dot{r}_{\mathrm{Elc}}(z)}{l \cdot A_{\mathrm{Fu}}}; \quad \times \quad z \in [0, l) \tag{26}$$

$$\frac{dc_{Fu}(z, CH_4)}{dt} + u_{Fu}(l)\frac{\partial c_{Fu}(z, CH_4)}{\partial z_c} = \frac{-\dot{r}_{Ref(I)}(z)}{l \cdot A_{Fu}}; \quad z \in [0, l) \tag{27}$$

$$\frac{dc_{Fu}(z, C_2H_5OH)}{dt} + u_{Fu}(l)\frac{\partial c_{Fu}(z, C_2H_5OH_4)}{\partial z_c} = \frac{-\dot{r}_{Ref(II)}(z)}{l \cdot A_{Fu}}; \times \quad z \in [0, l) \tag{28}$$

$$\frac{dc_{Fu}(z, H_2O)}{dt} + u_{Fu}(l)\frac{\partial c_{Fu}(z, H_2O)}{\partial z_c} = \frac{-\dot{r}_{Ref(I)}(z) - \dot{r}_{Ref(II)}(z) - \dot{r}_{Shi}(z) + \dot{r}_{Elc}(z)}{l \cdot A_{Fu}}; \times \quad z \in [0, l) \tag{29}$$

$$\frac{dc_{Fu}(z, CO)}{dt} + u_{Fu}(l)\frac{\partial c_{Fu}(z, CO)}{\partial z_c} = \frac{\dot{r}_{Ref(I)}(z) + 2\dot{r}_{Ref(II)}(z) - \dot{r}_{Shi}(z)}{l \cdot A_{Fu}}; \times z \in [0, l) \tag{30}$$

$$\frac{dc_{Fu}(z, CO_2)}{dt} + u_{Fu}(l)\frac{\partial c_{Fu}(z, CO_2)}{\partial z_c} = \frac{\dot{r}_{Shi}(z)}{l \cdot A_{Fu}}; \quad z \in [0, l) \tag{31}$$

2.2.4. Electrochemical model

For SOFC, electrochemical models are coupled with heat and mass transfer models to determine the distribution of local current density and electrode over potentials inside the SOFC.

The relationship between cell current density and voltage is written as follows:

$$I = \frac{U_{ocp} - U_{op}}{R_{ohm} + R_{anode} + R_{cathode}} \tag{32}$$

where U_{ocp} is the function of SOFC operation temperature and gas partial pressure in anode and cathode, which can be regulated as follows:

$$U_{ocp} = U^0_{H_2} + \frac{RT}{2F}\ln\left(\frac{p_{f,H_2}(p_{a,O_2})^{0.5}}{p_{f,H_2O}}\right) + \frac{RT}{4F}\ln\left(\frac{1}{p_{std}}\right) \tag{33}$$

where

$$U^0_{H_2} = 1.2723 - 2.7645e - 4 \times T \tag{34}$$

$U^0_{H_2}$ is the ideal voltage for hydrogen oxidization [19]. p_{std} is the standard pressure.

The output power density of SOFC can be calculated by:

$$P_{SOFC} = U \times I \tag{35}$$

As both electrodes are normally good conductors, a constant cell operation voltage U_{op} throughout the cell is normally considered [20].

Ohmic losses are caused by resistance to conduction of ions and electrons, and contact resistance between cell components.

$$R_{ohm} = \rho_e\delta_e + \rho_c\delta_c + \rho_a\delta_a \tag{36}$$

The activation polarization terms are controlled by the electrode reaction kinetics of the respective electrodes. They represent voltage loss incurred due to the activation necessary for charge transfer. Over potentials at the cathode and anode are assumed independent of the local current density. The model derived by Achenbach is adopted in this paper [21].

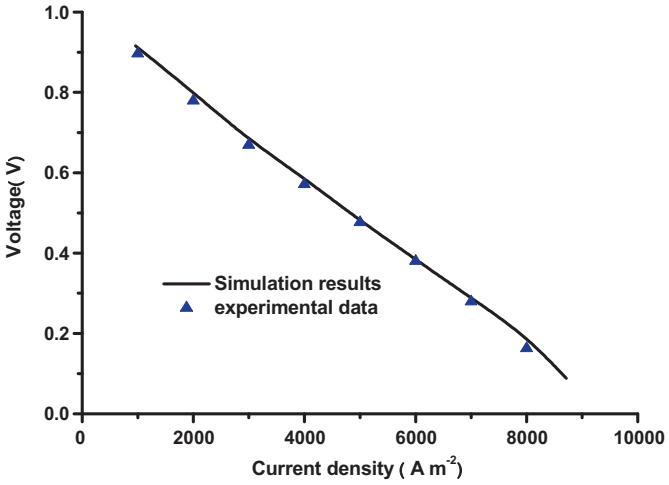

Fig. 3. CH_4 fueled SOFC model validation.

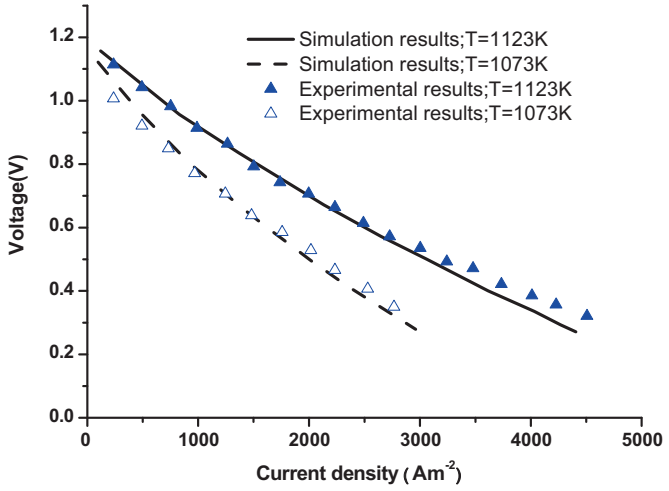

Fig. 4. C_2H_5OH fueled SOFC model validation.

2.2.5. Model validation

The SOFC model developed in this paper is validated using the experimental data published in Ref. [22]. The input parameters and fuel utilization values of the experimental data were simulated with the model, giving voltage and power as results. Input parameters and results are shown in Table 2. The simulation results match both experimental data1 and experimental data 2 with errors of only 1.01 and 1.09%, respectively.

In order to further validate the SOFC sub-model, the polarization curves generated by the simulation model are compared with experimental ones for different fuels as shown in Figs. 3–5. Results shows that the developed model can achieve errors lower than 3%. Unfortunately, we have not acquired the SOFC stack experimental data, so the validation of the stack performance is not yet possible. CH_4 fueled SOFC sub-model was validated by experimental data published in [23]. C_2H_5OH fueled SOFC sub-model was validated with experimental results with the operating temperature at 1123 K and 1073 K published in [24]. H_2 fueled SOFC sub-model was validated with experimental data from Siemens published in [25].

2.3. Gas turbine model

The micro gas turbine selected in this paper is C30 from CAPSTONE, which is a single-shaft micro gas turbine equipped with

Table 2
Validation of the SOFC model.

	Experimental data 1	Simulation results	Experimental data 2	Simulation results
Pressure (bar)	1.05	1.05	3.5	3.5
Fuel flow rate (mol/s)	1.511×10^{-3}	1.511×10^{-3}	2.287×10^{-3}	2.287×10^{-3}
Air flow rate (mol/s)	1.055×10^{-2}	1.055×10^{-2}	1.29×10^{-2}	1.29×10^{-2}
Inlet fuel temperature	823 K	823 K	860 K	860 K
Inlet air temperature	1104 K	1104 K	1048 K	1048 K
Fuel utilization	69%	69%	69%	69%
Inlet fuel composition (mole fraction)				
H_2	25.8%	25.8%	22.6%	22.6%
H_2O	28.4%	28.4%	33.4%	33.4%
CH_4	11%	11%	13.1%	13.1%
CO	5.7%	5.7%	5.7%	5.7%
CO_2	22.8%	22.8%	24.1%	24.1%
N_2	6.3%	6.3%	1.1%	1.1%
Results				
Voltage (V)	0.69	0.697	0.639	0.632
Power (W)	104.8	105.86	157	155.28
Error	–	1.01%	–	1.09%

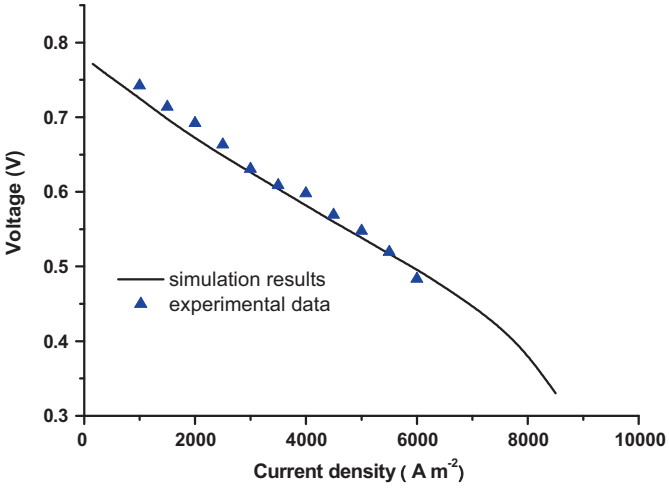

Fig. 5. H_2 fueled SOFC model validation.

a centrifugal compressor and a radical turbine. Major parameters of C30 gas turbine are summarized in Table 3. The compressor and turbine models provide the standard thermodynamic equations for the input-output relationship of the working fluid based on pressure ratio and isentropic efficiency, as shown in Table 4. The latter values are determined by a performance map, which describes the compressor and turbine by introducing pressure and efficiency as a function of mass flow rate and shaft speed. Performance maps of the compressor are shown in Fig. 6.

Table 3
Parameters of the C30 gas turbine at design point.

Parameters	Value
Pressure ratio	3.2
Compressor isentropic efficiency	80%
Air flow rate	0.31 kg s^{-1}
Fuel flow rate	0.0024 kg s^{-1}
Turbine inlet temperature	1173K
Turbine isentropic efficiency	90%
Turbine exit temperature	548 K
Turbine exit pressure	103 KPa
Recuperator effectiveness	90%
Electric power generated	30 kW
Electric efficiency	26%

Table 4
Thermodynamic equations for compressor and turbine models.

Compressor outlet pressure	(37) $P_{out} = \varepsilon P_{in}$
Compressor outlet temperature	(38) $T_{c,out} = T_{c,in} + T_{c,in}(\pi^{(k-1)/k} - 1)/\eta_c$
Compressor consumed power	(39) $W_c = 4.18 c_p G_k T_{c,in}(\varepsilon^{(k-1)/k} - 1)/\eta_c$
Turbine outlet temperature	(40) $T_{t,out} = T_{t,in}\left(\frac{P_{t,out}}{P_{t,in}}\right)^{(K_T-1)/K_T}$
Turbine output power	(41) $W_c = 4.18 c_{p,R} G_T T_{t,in}\left[1 - \left(\frac{P_{t,out}}{P_{t,in}}\right)^{(K_T-1)/K_T}\right]\eta_t$

Generator efficiency in this paper is assumed constant. The power output from the gas turbine can be calculated by:

$$W_{GT} = \eta_{gen}(\eta_t W_t - W_c) \quad (42)$$

where η_{gen} is the generator efficiency, η_t is the turbine mechanical efficiency, and W_t, W_c are turbine output power and compressor consumed power, respectively.

2.4. Combustor model

Assume that all residual combustible compounds such as C_2H_5OH, CH_4, CO, and H_2 formed in the fuel cell stack could be fully oxidized in the combustor. The associated chemical reactions are as follows:

$$C_2H_5OH + 3O_2 = 2CO_2 + 3H_2O + \Delta H_{rxn,CH_4} \quad (43)$$

$$CH_4 + 2O_2 = CO_2 + 2H_2O + \Delta H_{rxn,CH_4} \quad (44)$$

$$CO + \frac{1}{2}O_2 = CO_2 + \Delta H_{rxn,CO} \quad (45)$$

$$H_2 + \frac{1}{2}O_2 = H_2O + \Delta H_{rxn,H_2} \quad (46)$$

The temperature of the product gas (T_p) can be calculated based on a simple energy balance on the combustor control volume.

$$\sum_i h_{r,i} + \Delta h_{rxn,C_2H_5OH} + \Delta h_{rxn,CH_4} + \Delta h_{rxn,CO} + \Delta h_{rxn,H_2} = \sum_j n_j \int_{T_r}^{T_p} c_{p,i} dT \quad (47)$$

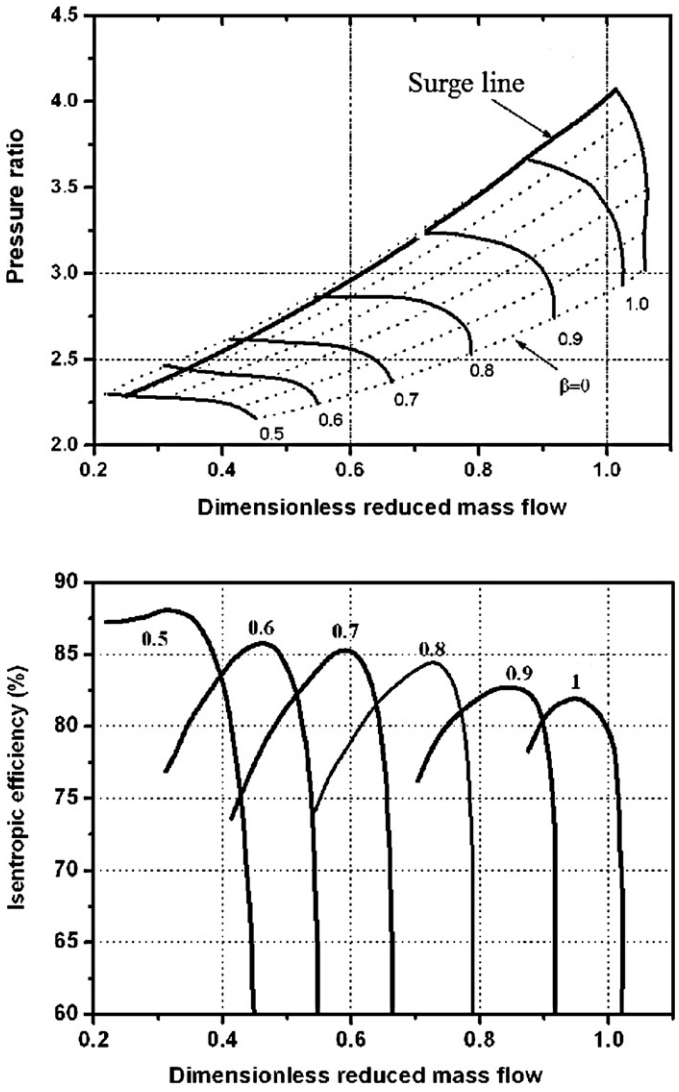

Fig. 6. Performance maps of compressor.

2.5. Heat exchange model

The heat exchanger model presented in this paper is simulated based on the ε-*NTU* method [26], implementing temperature-dependent specific heat.

An iterative procedure is implemented to assess the outlet temperatures, based on the calculation of average hot and cold fluid-specific heats. These parameters depend on the unknown HE outlet temperature. Thus, estimated values for the temperatures are selected, allowing for the calculation of average specific heats and consequently, through the ε-*NTU* method, the outlet temperature is re-calculated. The procedure is stopped when the convergence criterion on such temperature is satisfied.

3. Results and discussion

3.1. System performance

3.1.1. Performance at design point

The hybrid system operation parameters at design points fed by methane, hydrogen, and ethanol are shown in Table 5. Fig. 7 shows the process parameters at design points of the hybrid system operating with all three fuels. To evaluate the performance of the system fed by new fuel, new design points must be defined for each fuel at first. The gas turbine is only slightly influenced by the fuel choice, thus, the original air flow rate from the methane-fueled system is chosen. SOFCs are the most important component in the system, contributing most of the net power. To make SOFCs operate at their design point, the fuel flow for each new fuel is designed with the objective of reaching the same SOFC operating temperature as with methane, which is 1273 K.

Table 5
Design parameters of hybrid system.

Parameters	Methane	Hydrogen	Ethanol
n_{fuel} (mol s^{-1})	0.2996	0.767	0.1708
n_{air} (kg s^{-1})	0.31	0.307	0.34
P_{net} (kW)	150	105	132
I (A m^{-2})	2980	1910	2532
TIT (K)	1173	1069	1132
T_{MEA} (K)	1273	1273	1273
γ_{SC}	2	–	1.7
π_c	3.2	3.04	3.13
η_{net}	62.29%	56.59%	60.5%

When the hybrid system is operating with hydrogen, the design calculation returns a fuel flow rate of 0.767 mol s^{-1}, 2.56 times more than that of methane. Assuming that fuel utilization is constant, this value corresponds to an SOFC current density of only 1910 A m^{-2}. The reason for the changed relationship between SOFC design current density and operating temperature is the lack of cooling effect from steam reforming. Higher air flow rate should be required for the hydrogen-fed hybrid system to reach the original design current density at an acceptable temperature level. The reduction current implies a reduction of design power to 0.7 of the value reached with methane. The net efficiency is reduced to 56.59%. The lower efficiency is due to the higher cooling air demand per power, and thus higher heat loss. The same effect has been observed by other researchers [27].

The design calculation for ethanol fuel returns a relative fuel flow rate of 57% of the methane value, that is, 0.1708 mol s^{-1}. With higher molar hydrogen yield of ethanol, this value corresponds to an SOFC current density of 2549 A m^{-2}. The changed relationship between SOFC temperature and current density is caused by lower specific heat per mole of hydrogen required by the reforming reaction. The reduced current density implies a reduction of net power to 88% of the value reached with methane fuel, at a net efficiency of 60.5%. These results are achieved based on the assumption that ethanol vaporization is accomplished by exhaust gas heat. If an electric heater is used for this purpose, the net power will decrease to 80.02% of the methane value and the net efficiency will decrease to 55.4%.

3.1.2. Part-load performance

In the SOFC-GT hybrid system, SOFC is the most important component that contributes most of the net power. To make SOFC operate at its design point, a part-load strategy with a constant SOFC mean MEA temperature is pursued in this paper.

Fig. 8 shows the major parameters and system performance of the SOFC-GT hybrid system operating with methane at part-load conditions. The lowest electrical power of 21% of the designed value (31.5 kW) can be achieved by reducing the air and fuel flow rates at constant SOFC operating temperature. At partial load operation, less fuel is fed into the SOFC stack while the fuel utilization is assumed constant. Consequently, the unreacted fuels in SOFC exhaust decreases, determining the reduction of turbine inlet tem-

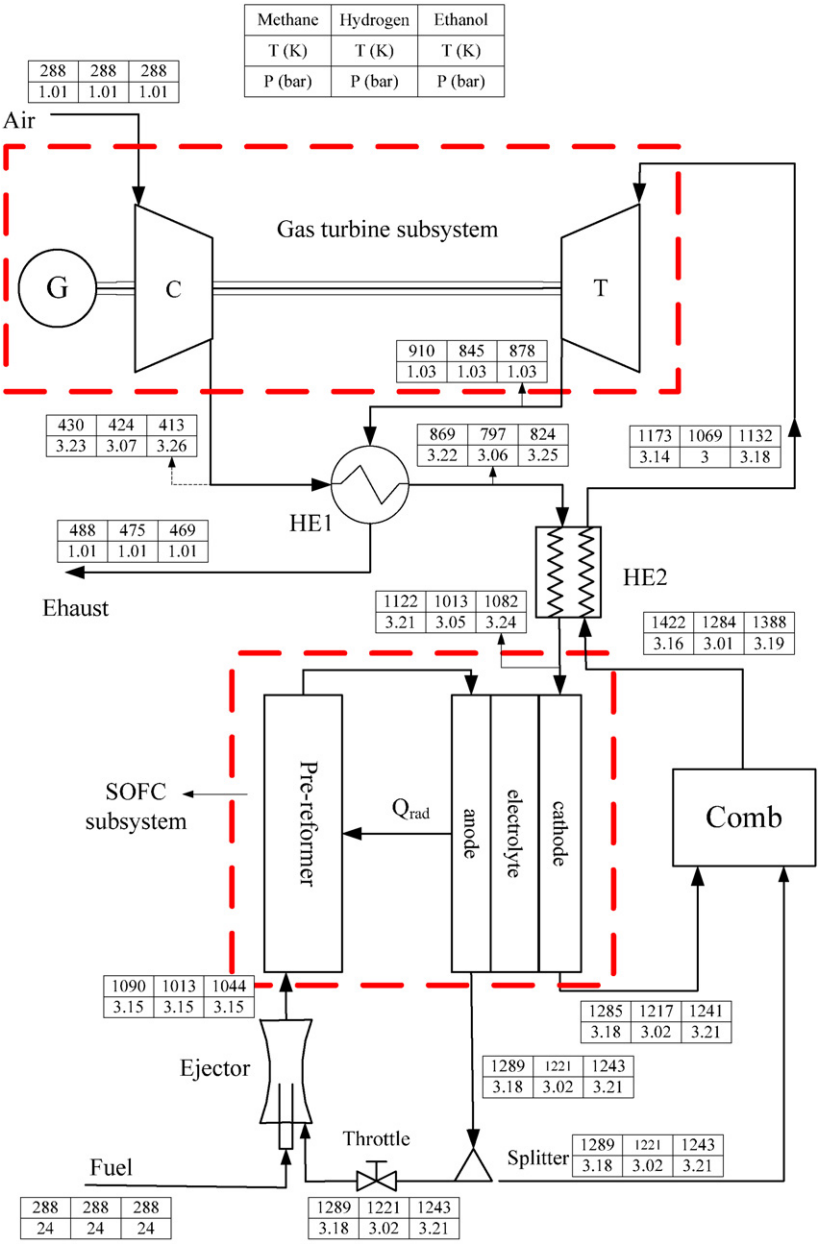

Fig. 7. Process parameters of hybrid system at design point.

perature. The variation of the gas turbine air flow rate and the reduction of turbine inlet temperature (TIT) cause the reduction of both GT output power and efficiency. On the other hand, an increase in cell voltage is obtained because of the current density reduction caused by the reduction of the fuel flow rate. The high voltages achieved by the cell determine the lower efficiency defects of the SOFC stack. These effects are in contrast, which cause the system efficiency to be in a steady-state ranging from 59.6% at minimum load to a maximum of 65.8% at intermediate load (59% power), and back to 62.6% at the design point. For the SOFC tube, the minimum MEA temperature has a sharp bend at 68% power, where the maximum MEA temperature is lowest at 1294 K. The highest local gradient in radial direction occurs at the design point with 797 K m^{-1}, caused by the higher cooling effect of the fuel reforming reaction.

Fig. 9 shows the major parameters and system performance of the SOFC-GT hybrid system operating with hydrogen at part-load conditions. The electrochemical power of the hybrid system can be produced in the range 14–70% of the value reached with methane, that is, 21–105 kW. Compared with the operation parameters for the methane-fueled system, the strongest difference is the maximum radial temperature gradient, which for a certain power output (105 kW, 70% of the design power with methane), is approximately three times higher for the methane system. For both options, the maximum radial gradient occurs at the cell bottom, where air and fuel meet at either side of the MEA with different temperatures. Due to the absence of an endothermic-reforming reaction, the temperature of the entering fuel is higher than if methane is used and the difference to the air is thus lower. The turbine inlet temperature is lower with hydrogen fuel caused by lower SOFC exhaust temperature, both at equal power and air flow rate are compared. This causes the gas turbine to be operating on a different line with a methane-based system.

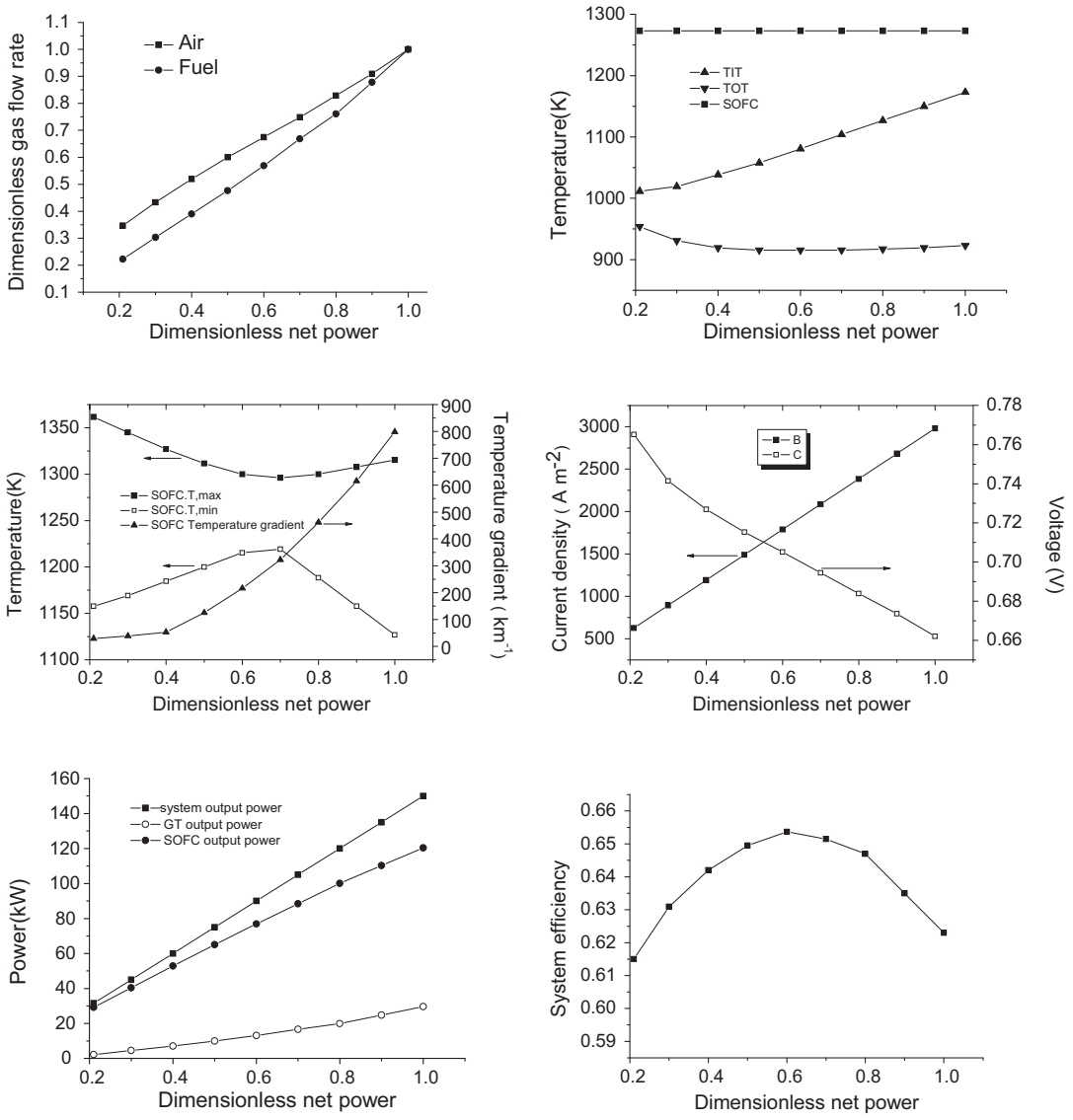

Fig. 8. Electrochemical performance and operation parameters of SOFC-GT hybrid system fed by methane.

Fig. 10 shows the major parameters and system performance of an SOFC-GT hybrid system operating with ethanol at part-load conditions. Net power output is in the range of 19–88% of power reached by methane-based system at design point. At 88% power, the net efficiency is 60.5%, lower than the value at 88% power by methane system, that is, 63.7%. Similar to the hydrogen-fed system, the ethanol fuel also slightly reduced the thermal load to the fuel cell, as the maximum local MEA temperature is lower, and the minimum MEA temperature is higher than that for the methane case. At 88% power, the maximum radial temperature gradient is approximately 40% lower than that of methane, which is a consequence of the lower heat consumption of the reforming reaction. The turbine inlet temperature is higher than that of H_2, but lower than that of methane at equal net power output.

Fig. 11 shows the gas turbine operational line in the compressor map. Although the air flow rate decreases with the reduction of system output power, the reduction of TIT, which causes a pressure ratio decrease, ensures that the compressor surge will not occur during the system off-design operation range for all fuels.

3.2. Measures to increase power output for non-designed fuel

To increase the power output of the hybrid system operating with non-designed fuel, the following measures were introduced and investigated in steady-state.

- Case 1: Using the auxiliary fuel to improve the TIT to its design value.
- Case 2: Exhaust gas bypassing the HE1 to decrease heat recuperation.
- Case 3: Exhaust gas bypassing the HE1 and using auxiliary fuel.

As discussed in Section 3.1.1, the hydrogen-fed SOFC-GT hybrid system can only output 70% of the design power with normal part-load strategy. In the present paper, we take the system fed by hydrogen to explain the three cases considering its lowest net power output. Fig. 12 shows the minimum and maximum power and efficiency curves of the discussed measure. Fig. 12 shows the power output of the hybrid system operating with different cases.

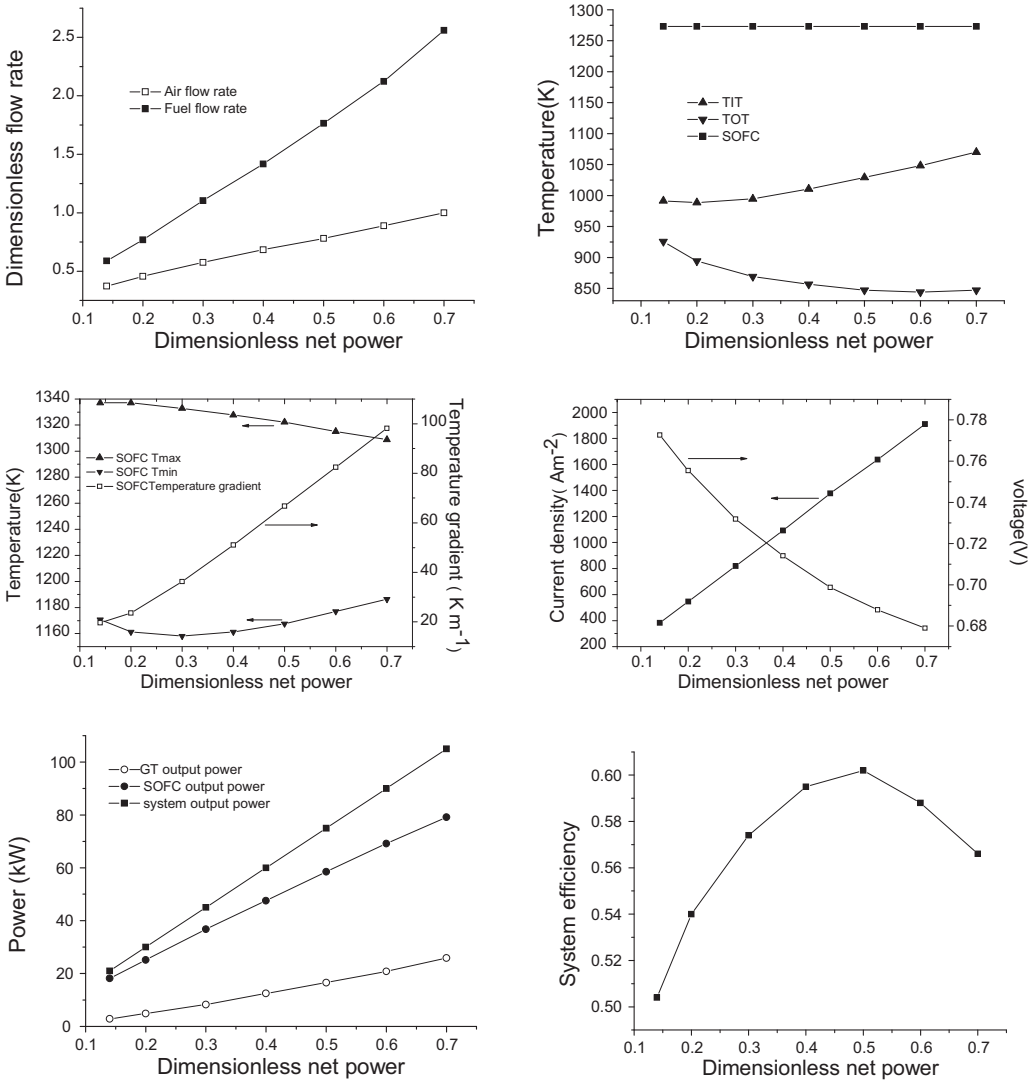

Fig. 9. Electrochemical performance and operation parameters of SOFC-GT hybrid system fed by hydrogen.

- Case 1: As the turbine inlet temperature is below its design value, auxiliary firing upstream the turbine could significantly increase the GT power output. An attempt has been made by adding auxiliary fuel flow such that the relationship between turbine inlet temperature and air flow equals the methane fuel case. At the design flow rate, to lift the TIT to 1173 K, appropriately 15% of the fuel was directly fed to the combustor. However, burning fuel generally increases heat production; thus, the SOFC fuel utilization must be decreased to keep the temperature constant. The simulation shows that with this method, the power can only be increased insignificantly to 72.6% as shown in Fig. 13.
- Case 2: To decrease heat recuperation, part of the exhaust can be bypassed around the HE1 by using the bypass valve. The simulation shows that this method can increase the power output at the design SOFC operating temperature to a value of 84% of the methane design net power if 70% of the exhaust gas is bypassed as shown in Fig. 13. However, net efficiency decreased to 48%, caused by the higher exhaust temperature. The turbine inlet temperature decreased further, which led to less power contribution of the gas turbine.
- Case 3: If 70% of the exhaust gas is bypassed and the TIT is increased to its original design value of 1173 K with auxiliary firing, a net power output of appropriately 94% of methane design value can be achieved, as shown in Fig. 13. Net efficiency, however, decreased to 45%.

Case 3 proved it could increase the power output almost to its original, methane-based value, at the cost of significant power efficiency. A promising control strategy for a system mainly operating at part-load would be to operate normally with a closed bypass valve, and without auxiliary fuel up to a power of 70%, and for a higher power to gradually open the bypass and introduce fuel to the combustor directly. To implement this strategy, the exhaust gas bypass and the auxiliary fuel flow must be integrated into the operating control strategy. Assuming a digital control unit, this does not imply any hardware modification.

Fig. 14 shows the compressor operation line of different cases. Higher turbine inlet temperature with Case 1 and Case 3 are acquired with auxiliary fuel, which caused a higher pressure ratio at a constant air flow rate. Therefore, the surge margin is decreased but does not cross the surge line; thus, the gas turbine operation is safe. Net power produced by the gas turbine is higher than that of Case 2 and normal operation. In Case 2, TIT is decreased rapidly due to the bypass valve, which makes the compressor surge mar-

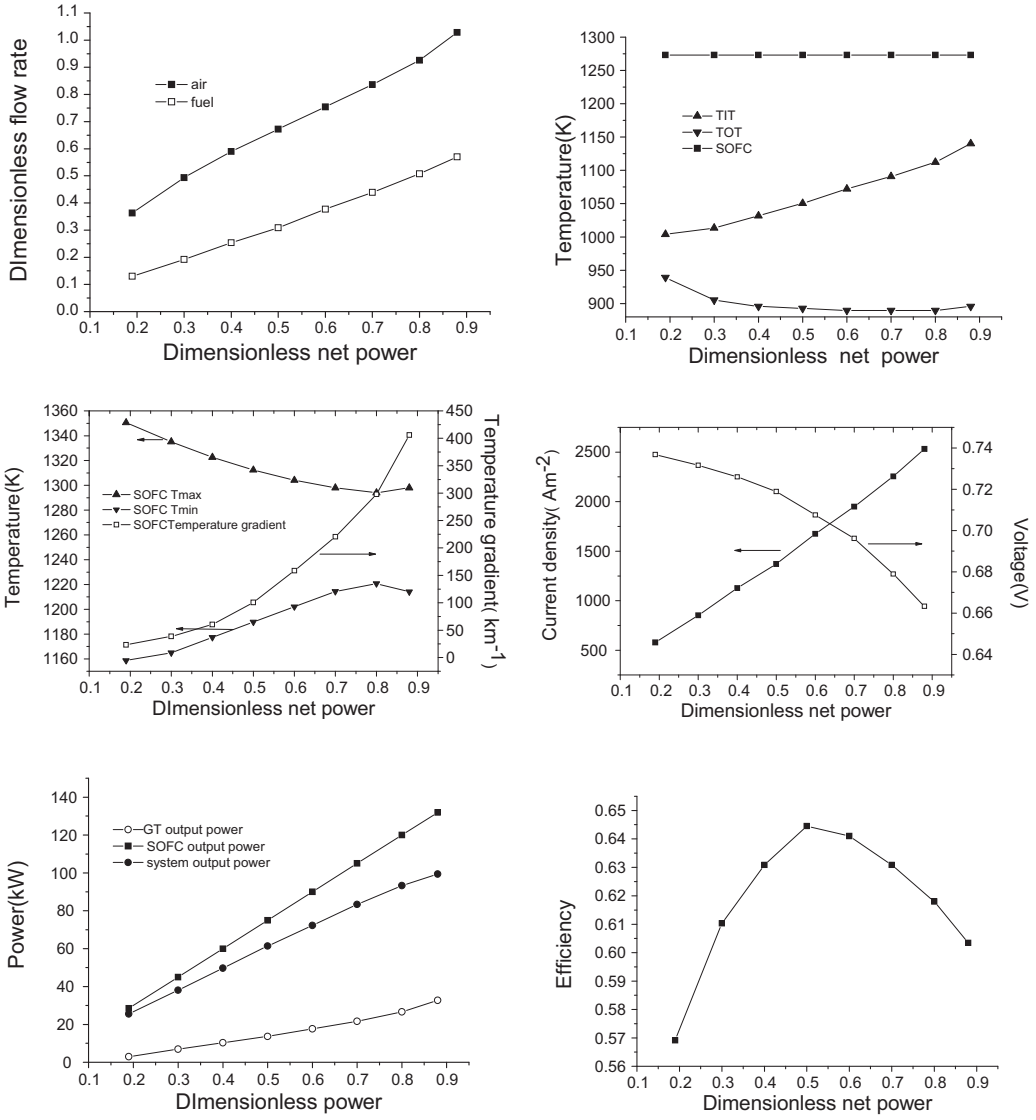

Fig. 10. Electrochemical performance and operation parameters of SOFC-GT hybrid system fed by ethanol.

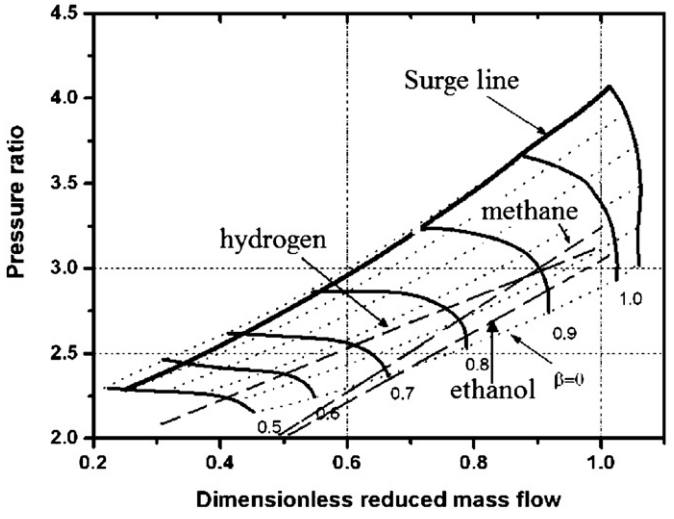

Fig. 11. Gas turbine operational line with different fuels at part load operations.

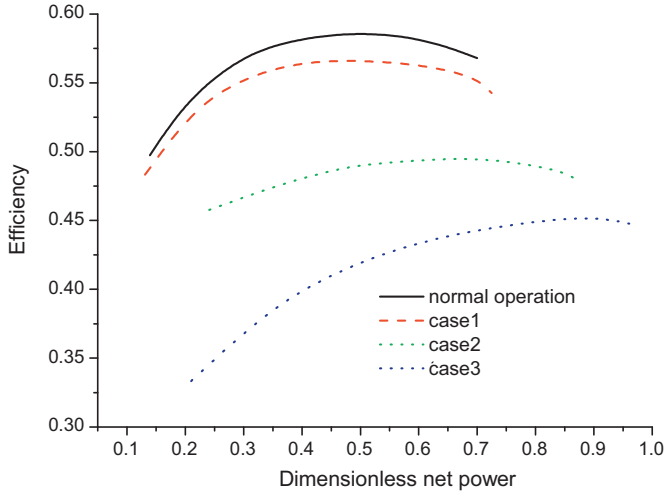

Fig. 12. Enhancing power output for the hydrogen fueled system with different methods.

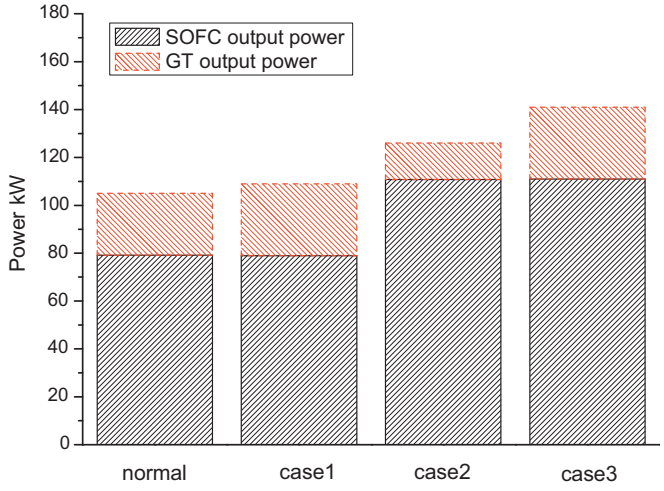

Fig. 13. Gas turbine operation line with different enhancing power cases.

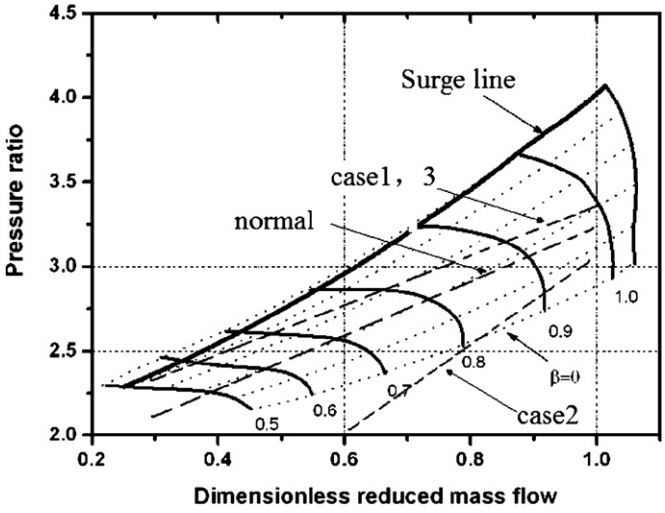

Fig. 14. Power output of hybrid system operating with different cases.

gin increase at part-load operation. However, gas turbine output power is thus reduced to a low level as shown in Fig. 13.

4. Conclusions

The performance of an SOFC-GT hybrid system designed for methane fuel operating with other suitable fuels was analyzed. New design points were defined for each fuel. At new design points, the net electric efficiencies are 62.29, 56.59, and 60.5, for methane, hydrogen, and ethanol, respectively.

The maximum output power of the system fueled by hydrogen will decrease to 105 kW (70% of the methane value) due to lack of cooling by stream reforming. Due to the absence of endothermic reforming reactions, the maximum radial temperature gradient is much higher than that of the methane system.

When the system is fueled by ethanol, the net output power will decrease to 88% of the methane value due to the lower cooling effect of stream reforming. However, with increased heat recuperation from the gas turbine exhaust gas, the net efficiency can remain at 60.5% at a high level. This result is based on the assumption that ethanol vaporization is accomplished by exhaust gas heat. If an electric heater was used for this purpose, the net power would be reduced to 80.02% of the methane value and the net efficiency will decrease to 55.4%.

To increase the power output of the hybrid system operating with non-designed fuel, three possible measures are introduced in this paper. Simulation results show that for a hydrogen-fueled system, simply using the auxiliary fuel to improve the TIT to its design value cannot increase the system output power significantly, while bypassing gas exhaust around HE1 can increase the net output power to 84% of the methane designed power. When both measures are adopted at the same time, the net output power will increase to 94% of methane-designed power. However, the net efficiency will decrease to 45%.

Acknowledgments

This project was supported by National Basic Research Program of China (973 Program) under the contact number 2010CB227301.

References

[1] U.S. DOE, Fuel Cell Handbook, 7th ed., DOE/NETL, Morgantown WV, 2004.
[2] S.K. Park, T.S. Kim, J. Power Sources 163 (2006) 490–499.
[3] Lijin Wang, Huisheng Zhang, Shilie Weng, J. Power Sources 177 (2008) 579–589.
[4] Aiguo Liu, Yiwu Weng, J. Power Sources 195 (2010) 204–213.
[5] F. Calise, A. Palombo, L. Vanoli, J. Power Sources 158 (2006) 225–244.
[6] P. Aguiar Iora, C.S. Adjiman, N.P. Brandon, Chem. Eng. Sci. 60 (2005) 2963–2975.
[7] Jan Van Herle, F. Marechal, S. Leuenherger, D. Favrat, J. Power Sources 118 (2003) 372–383.
[8] R. Suwanwarangkul, E. Croiset, E. Entchev, S. Charojrochkul, M.D. Prizker, et al., J. Power Sources 161 (2006) 308–322.
[9] Siamak Farhad, Feridun Hamdullahpur, Yeong Yoo, Int. J. Hydrogen Energy 35 (2010) 3758–3768.
[10] M. Jenner, T. Dork, A. Schuler, Proceeding of the Fifth European Solid Oxide Fuel Cell Forum, Lucene, Switzerland, 2002.
[11] Y. Yi, A.D. Rao, J. Brouwer, G.s. Samuelsen, J. Power Sources 144 (2005) 67–76.
[12] Xinjian-Zhu Bo Huang, Wan-Qi Hu, Qing-Chun Ye, Heng-Yong Tu, J. Power Sources 86 (2009) 29–36.
[13] Jens Palsson, Azra Selimovic, Lars Sjunnesson, J. Power Sources 86 (2000) 442–448.
[14] SCE/SW, SCE/SW former 25 kW SOFC project on logistic fuel study. 1995, Southern California Edison/Siemens Westinghouse.
[15] AAVV, in: Gregors Hoogers (Ed.), Fuel Cell Technology Handbook, CRC Press, 2003.
[16] P. Aguiar, C.S. Adjiman, N.P. Brandon, J. Power Sources 138 (2004) 120–136.
[17] Meng Ni, Dennis Y.C. Leung, Michael K.H. Leung, Int. J. Hydrogen Energy 32 (2007) 3238–3247.
[18] Akande Abayomic, Ahmed Aboudheir, Raphael Idem, Ajay Dalai, Int. J. Hydrogen Energy 31 (2006) 1707–1715.
[19] S. Campanari, P. Iora, J. Power Sources 132 (2004) 113–126.
[20] P. Augiar, C.S. Adjiman, N.P. Brandon, J. Power Sources 138 (2004) 120–136.
[21] E. Achenbach, J. Power Sources 49 (1994) 338–348.
[22] S. Campanari, P. Lora, J. Power Sources 132 (2004) 113–126.
[23] W.A. Rogers, R.S. Gemmen, C. Johnson, M. Prinkey, M. Shahnam, Fuel Cell Sci. Eng. Technol. ASME (2003) 517–520.
[24] B. Huang, X.J. Zhu, W.Q. Hu, Y Q.C., H.Y. Tu, J. Power Sources 186 (1) (2009) 29–36.
[25] B. Huang, X.J. Zhu, W.Q. Hu, Q.C. Y, H.Y. Tu, J. Power Sources 186 (1) (2009) 29–36.
[26] Compact Heat Exchanger, 3rd ed., Kays, London, 1998.
[27] S.H. Chan, C.F. Low, O.L. Ding, J. Power Sources 103 (2002) 188–200.